Biosensors and Bioelectronics 169 (2020) 112618

Contents lists available at ScienceDirect

Biosensors and Bioelectronics

journal homepage: http://www.elsevier.com/locate/bios

Ad hoc hybrid synaptic junctions to detect nerve stimulation and its application to detect onset of diabetic polyneuropathy

Sujasha Gupta [a,1], Subhadip Ghatak [b,1], Travis Hery [a], Savita Khanna [b], Mohamed El Masry [b,c], Vishnu Baba Sundaresan [a,*], Chandan K. Sen [b,**]

[a] Department of Mechanical and Aerospace Engineering, The Ohio State University, Columbus, OH, 43220, USA
[b] Indiana Center for Regenerative Medicine and Engineering, Indiana University School of Medicine, Indianapolis, IN, 46202, USA
[c] Plastic and Reconstructive Surgery Department, Zagazig University, 44519, Egypt

ARTICLE INFO

Keywords:
Synaptic transistor
Neuronal-electronic interface
High bandwidth action potential sensor
Polyneuropathy

ABSTRACT

We report a minimally invasive, synaptic transistor-based construct to monitor in vivo neuronal activity via a longitudinal study in mice and use depolarization time from measured data to predict the onset of polyneuropathy. The synaptic transistor is a three-terminal device in which ionic coupling between pre- and post-synaptic electrodes provides a framework for sensing low-power (sub μW) and high-bandwidth (0.1–0.5 kHz) ionic currents. A validated first principles-based approach is discussed to demonstrate the significance of this sensing framework and we introduce a metric, referred to as synaptic efficiency to quantify structural and functional properties of the electrodes in sensing. The application of this framework for in vivo neuronal sensing requires a post-synaptic electrode and its reference electrode and the tissue becomes the pre-synaptic signal. The ionic coupling resembles axo-axonic junction and hence we refer to this framework as an ad hoc synaptic junction. We demonstrate that this arrangement can be applied to measure excitability of sciatic nerves due to a stimulation of the footpad in cohorts of m^+/db and db/db mice for detecting loss in sensitivity and onset of polyneuropathy. The signal attributes were subsequently integrated with machine learning-based framework to identify the probability of polyneuropathy and to detect the onset of diabetic polyneuropathy.

1. Introduction

Neural membrane opens to allow positively charged ions inside the cell and negatively charged ions out giving rise to action potential. As part of the sequelae, the positive charge of the nerve fiber rises sharply to reach +40 mV allowing the impulse to conduct down the nerve fiber. A series of action potentials allows the electrical impulse to propagate down the nerve. Under conditions of pathophysiology such as diabetic polyneuropathy, varying degrees of nerve conduction changes appear in the early asymptomatic stage (Erdogan et al., 2011). Electrophysiological abnormality as manifested by abnormal nerve conduction signal parameters i.e., conduction velocity vs. amplitude of the compound action potential is a hallmark of diabetic polyneuropathy. In db/db mice, weakening of compound motor action potential (CMAP) in the hind paw has been reported in response to stimulation of sciatic nerves (Heise et al., 2012). Analytically, nerve conduction studies are performed by applying depolarizing square wave electrical pulses to the skin over a peripheral nerve. Such exogenous supraphysiological stimulation generates sensory nerve action potential that is recorded at a point further along that nerve.

The diagnosis of structural damage in neuropathy can be classified into two broad groups – (a) quantitative sensory testing and (b) imaging. Quantitative sensory testing, also referred to as nerve conductivity study (NCS) performed via Semmes-Weinstein monofilament (SWM) or pressure-specified sensory device (PSSD), is subjective and influenced by various attributes such as location of damage, body fat, skin surface preparation and does not provide sufficient resolution to detect early onset of polyneuropathy (Zhang et al., 2014). Although often combined with electromyography (EMG) that uses global response to detect localized defects in a nerve, such NCS technique has poor reproducibility and sensitivity to small structural damage. Imaging methods to detect structural damage in nerve fibers include ultrasound (US) imaging and

* Corresponding author.
** Corresponding author.
E-mail addresses: sundaresan.19@osu.edu (V.B. Sundaresan), cksen@iu.edu (C.K. Sen).
[1] These authors contributed equally to this study.

https://doi.org/10.1016/j.bios.2020.112618
Received 22 June 2020; Received in revised form 21 August 2020; Accepted 14 September 2020
Available online 21 September 2020

confocal microscopy. Among the two imaging methods, US imaging offers a non-invasive point of care approach with little or no patient education required prior to testing. Despite this advantage, US imaging suffers from poor resolution and cannot detect damage to small nerve fibers that are essential to detect the onset of peripheral neuropathy. Confocal imaging performed with molecular probes, is inapplicable at a point-of-care setting, and hence cannot be employed to routinely detect the onset, progression and repair of peripheral neuropathy (De Gregorio et al., 2018; Ruhdorfer et al., 2015). Nerve-interfacing electrodes such as the microelectrode array, flat interface nerve electrode and electrophysiology electrodes directly penetrate the nerve and result in tissue damage, repair and regeneration before being ready for use. In long term clinical studies, it is established that electrical signal attenuates over time and hence cannot be used in a longitudinal study for the detection of onset and progression of neuropathy (Gallardo et al., 2015; Kerasnoudis et al., 2015; Christensen et al., 2014). With estimates of about 5–10% of the general population and 50% of diabetics suffering from some form of neuropathy (retinal, peripheral) it is imperative to develop broadly applicable techniques that can detect damages to peripheral nerves to aid with early treatment and the discovery of novel therapeutics (Alshelh et al., 2016). The technical challenges in direct measurement of neuronal currents are due to the low power and high frequency structural components that attenuate rapidly within few 10s of microns. As discussed earlier, direct contact poses challenges due to tissue injury and immediacy of performing these measurements. Thus, any neuronal sensing framework should meet these contradicting requirements and provide high precision temporally accurate signal that mimics the action potential traveling through the nerve.

In this report, we demonstrate a sensing framework based on a three-terminal circuit where ionic currents between the input terminal and reference electrode affects redox current in a partially reduced conducting polymer used as the output terminal. This framework allows for measuring very small perturbations in the input terminal as a chronoamperometric response in the output terminal coupled by ionic capacitance of the volume enclosed between the three electrodes. By adjusting the geometrical attributes of the electrodes, ionic composition of the volume and capacitance of the conducting polymer in the output terminal, the coupling between the input and output terminal can be tailored to meet specified sensitivity, detection limit and spatial constraint. Owing to its structural resemblance to synaptic junctions, we refer to this architecture as a synaptic transistor, input and output terminals as pre-synaptic and post-synaptic terminals, and the volume enclosed between the electrodes as synaptic transistor cleft. For in vivo applications, the tissue under observation will become the pre-synaptic terminal and the chemoelectrical perturbations in the tissue will be pre-synaptic voltage and currents. The arrangement of components in the synaptic transistor and its application for in vivo sensing is shown in Fig. 1 (A-C). Our implementation of the synaptic transistor in this article uses conducting polymer electrodes for both the pre- and post-synaptic terminals as shown in Fig. 1A. A small voltage signal in the pre-synaptic electrode results in a current in the post-synaptic conducting polymer held at its partially reduced state. The post-synaptic current is observed due to the rapid ingress/egress of ions into/out of the conducting polymer to maintain electrochemical equilibrium with its environment. Owing to the properties of the synaptic transistor and partially reduced state of the post-synaptic terminal, we demonstrate the feasibility to detect cation concentration changes at a high bandwidth. (Fig. 1A, orange curve). A detailed physics of operation of this sensor is provided in SI 1.1. If this post-synaptic electrode is placed in vivo, the compound action potential passing through the sciatic nerve in response to a thermomechanical stimulus becomes the pre-synaptic input and the corresponding current in the conducting polymer electrode becomes the post-synaptic activity.

2. Experimental section

The conducting polymer used in this work is polypyrrole-doped with dodecylbenzenesulfonate due to its electronic-ionic coupling and biocompatibility (Gallego-Perez, 2017; Gupta et al., 2020). The polymer is formed on a 25 μm platinum wire and a 250 μm chloride silver wire reference electrode (Fig. 1B) is used as the quasi reference counter electrode (QRCE) for the construction of the synaptic transistor (Details on fabrication can be found in SI section 1.2). The synaptic transistor is enclosed in a 14G catheter and inserted obliquely at the back of the thigh (upper one-third region) parallel to the femur via hamstring muscles (approximately 5 mm above the knee) to reach a location proximate to the sciatic nerve. This choice was guided by the anatomical and technical challenges in precise repeated sensor placement over the

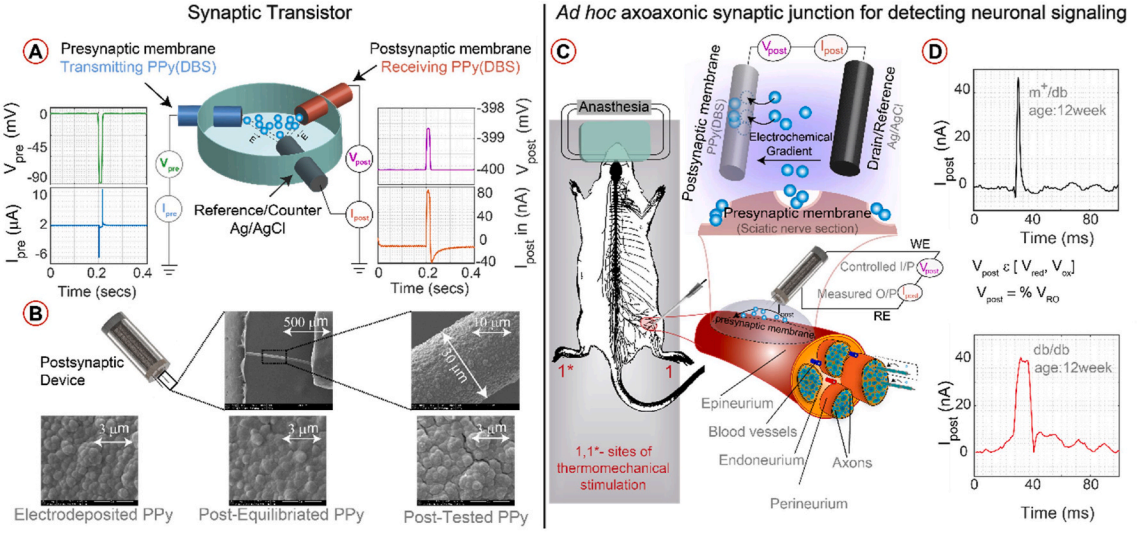

Fig. 1. The architecture for a synthetic synaptic transistor (shown in A) comprises of two identical conducting polymer electrodes (B) and a shared quasi counter reference electrode. The included volume between the three electrodes is analogous to a synaptic cleft and pre-synaptic stimulus (Vpre) causes a change to its ionic composition due to Ipre. The post-synaptic conducting polymer is held at a partially reduced state (Vpost = −400 mV) and change in post-synaptic current (Ipost) is a function of pre-synaptic stimulus magnitude and pre-synaptic membrane capacitance. The post-synaptic terminals are placed proximate to a nerve to form an ad hoc synaptic junction and is excitable due to neuronal communication(C). The measured Ipost (shown in D) is correlated to the neuronal communication and becomes a direct measure of sensitivity or lack thereof to touch.

approximate lifetime of the animal and the duration of this study. Sciatic nerve originates from lumbosacral region and extends to popliteal fossa and is widely selected to study the peripheral nerve injury and regeneration in animals (Bala et al., 2014). In this region, the span of the sciatic nerve is relatively superficial and can be easily accessed without damage to the muscle or surrounding structures. Alternatively, survival surgeries to access murine sciatic nerve at or above the gluteal region carry the risk of injury to deep structures and pelvic organs during repeated sensor reinsertions over the lifetime of the animal. Similarly, inserting the sensor via cannula at the level of popliteal fossa where sciatic nerve bifurcates into tibial and common peripheral nerves carries the risk of nerve injury due to the minimum muscle mass.

We should note that if one of the sensor electrodes touches the nerve, it leads to an electrical short leading to no signal. Presence/absence of this short can be confirmed using cyclic voltammetry (SI Fig. 12).

The sensor can be placed anywhere along the length of the sciatic nerve without affecting the measurements. This proximate arrangement of the sensor and the nerve leads to the formation of an ad hoc synaptic junction, where the compound action potential transmitted through the sciatic nerve in response to gentle touch forms the pre-synaptic input and the electrical current generated between PPy(DBS) and Ag/AgCl forms the post-synaptic output. The sensor placement is non-invasive to the nerve and allows the nerve to grow and mature following its normal course unlike contemporary methods that pierce into the tissue to interface with neurons (Cui et al., 2001; Malik, 2014; Tyler and Durand, 2003). The ionic coupling formed between the nerve, PPy(DBS) and the counter electrode resembles axoaxonic synaptic junction where one nerve terminal couples with the axon of another nerve to branch out a nerve signal (Cui et al., 2003). This sensing paradigm can be applied to any location to detect neuronal activity and does not require invasive physical contact with the neuron unlike all known neuronal sensors. Thus, the sensor detects as soon as the ad hoc synaptic junction is formed, and post-synaptic electrodes equilibrated in its environment (approximately 90–120 s to detect neuronal stimulation). A typical post-synaptic activity in diabetic db/db mice as measured by the synaptic transistor sensor in response to the same pre-synaptic input showed a slower and broader temporal resolution in post-synaptic activity in comparison to its non-diabetic littermate control (m^+/db) (Fig. 1D). The differences in temporal resolution is attributed to the kinetics of ion transport exchanged between the pre-synaptic (nerve) and post-synaptic (sensor) electrodes to support signal conduction through the nerve.

Faster signal conduction in a nerve is facilitated by hopping of ions (saltatory conduction) between Nodes of Ranvier (Luan et al., 2017). As the electrical impulse travels along the length of the sciatic nerve, enclosing bundle of axons, depolarization and repolarization of axons carries with it the resistive and capacitive electrical properties of the membranes encapsulating the axons. Myelin sheath, a fatty insulative layer on axons, facilitates quicker signal conduction by preventing current leakage as the signal travels only between Nodes of Ranvier. As the axons get demyelinated (capacitance increases), the saltatory conduction (ion hopping between Nodes of Ranvier) is impeded since the ionic current will require to travel more distance instead of utilizing the hopping sites. Prior electrophysiology studies have demonstrated an inverse relationship of specific nerve membrane capacitance to speed of conduction of electrical signals in neurons (Schmitz et al., 2001; Hodgkin and Huxley, 1952). Our simulation results of the synaptic transistor corroborate the same finding where we observed the dependence of temporal dynamics of post-synaptic current on capacitance of the pre-synaptic membrane. In this animal study, the sciatic nerve acts as the pre-synaptic membrane whereas the synaptic transistor sensor functions as the post-synaptic membrane and damage to the nerve's electrical properties, due to underlying neuropathic damage, is monitored using the temporal response of post-synaptic currents. Hence, by observing the temporal response of ionic current as sensed by the synaptic transistor sensor (depolarization time of post-synaptic currents; t_{DP}) and utilizing t_{DP} as a metric to detect the onset and progression of neuropathy, we were able to detect lowering of NCV in diabetic population as they progressively aged from week 7 to week 30.

3. Results and discussion

3.1. Synaptic transistor – characterization

We present a detailed characterization of the synthetic synaptic transistor to interpret current data from the post-synaptic circuit of the ad hoc synaptic junction formed around a nerve. The synthetic synaptic transistor is a three-electrode device (Fig. 1A) where PPy(DBS) electrodes and Ag/AgCl QRCE form the pre-synaptic and post-synaptic terminals. The stimulus to pre-synaptic terminal is varied between −100mV to +100 mV to vary the ionic composition of the synaptic cleft. The conducting polymer is held at x% of ΔV_{RO} ($\approx -400mV$) and responds to charge injection by the pre-synaptic terminal in the synaptic cleft. A typical post-synaptic response is shown (Fig. 1A) for a pre-synaptic stimulus of −50mV. We observe typical action potential attributes such as depolarization, hyperpolarization, and equilibration in the post-synaptic activity of the synthetic synaptic transistor. While different origins underlie the mechanism in the post synaptic terminal that leads to this response (**as explained in SI**), it is structurally similar and allows neuroscientists to interpret it much the same way as an action potential of neuronal origin. Owing to this similarity, we model the pre and post-synaptic circuits using FitzHugh-Nagumo (FHN) model (Fig. 2A). (Gentet et al., 2000; Waxman, 1980; Jacquir et al., 2006) The electrical equivalents (R, Z and L) are calculated following the description in SI (section 1.4.1) and the capacitance of the pre-synaptic PPy (DBS) is calculated from the filling efficiency (Kudryashov et al., 2018; Kumar et al., 2018). The cation egress (or) ingress from/into the cleft becomes an input to the post-synaptic circuit in addition to the post-synaptic potential (V_{post}). This pre-synaptic stimulus is converted into an equivalent electrical potential (Fig. 2C) using Gouy-Chapman model following the calculations shown in SI (section 1.4.2). The inputs together generate the post-synaptic activity and the model is calibrated to predict ionic conductance, depolarization and hyperpolarization current as a function of pre-synaptic stimulus (Fig. 2E). We also introduce synaptic efficiency (Fig. 2B) as a metric that indicates the strength of coupling between pre-synaptic and post-synaptic terminals as a ratio between the charge released by the pre-synaptic terminal and uptake by the post-synaptic terminal. We note that the synaptic efficiency averages between 36-40% and we note that future designs of the synaptic transistor can optimize the synaptic cleft volume to electrode area ratio to maximize this metric. The relationship between nerve membrane capacitance and the conduction velocity along its axon is known to have an inverse relationship (Northcutt and Sundaresan, 2015). Hence a parametric analysis was performed on the model to study the effect of pre-synaptic membrane capacitance (C_{pre}) on the post-synaptic current response. Simulation results from the model demonstrated that increasing C_{pre} lead to a slower release/intake of cations in the cleft, which affected the post-synaptic stimulus and its rate (see Fig. 2D right; where the black line with stimulus rate of 0.27 V/s corresponds to a membrane with $C_{pre} \sim 48$ μF and the grey line corresponds to $C_{pre} \sim 144$ μF). This affects the temporal response of I_{post} as can be observed in Fig. 2D (right-below). Notice a higher rise time (depolarization time; t_{DP}) for the membrane with higher capacitance. The rise time (t_{DP}) of post-synaptic current was noted for various C_{pre} values. A direct non-linear relationship between t_{DP} and C_{pre} was observed as summarized and shown in Fig. 2F. Thus, we establish the physics of operation of the synaptic transistor for neuronal sensing and use the temporal dynamics of post synaptic element in our longitudinal study to determine the onset, progression and loss of sensitivity in diabetic mice.

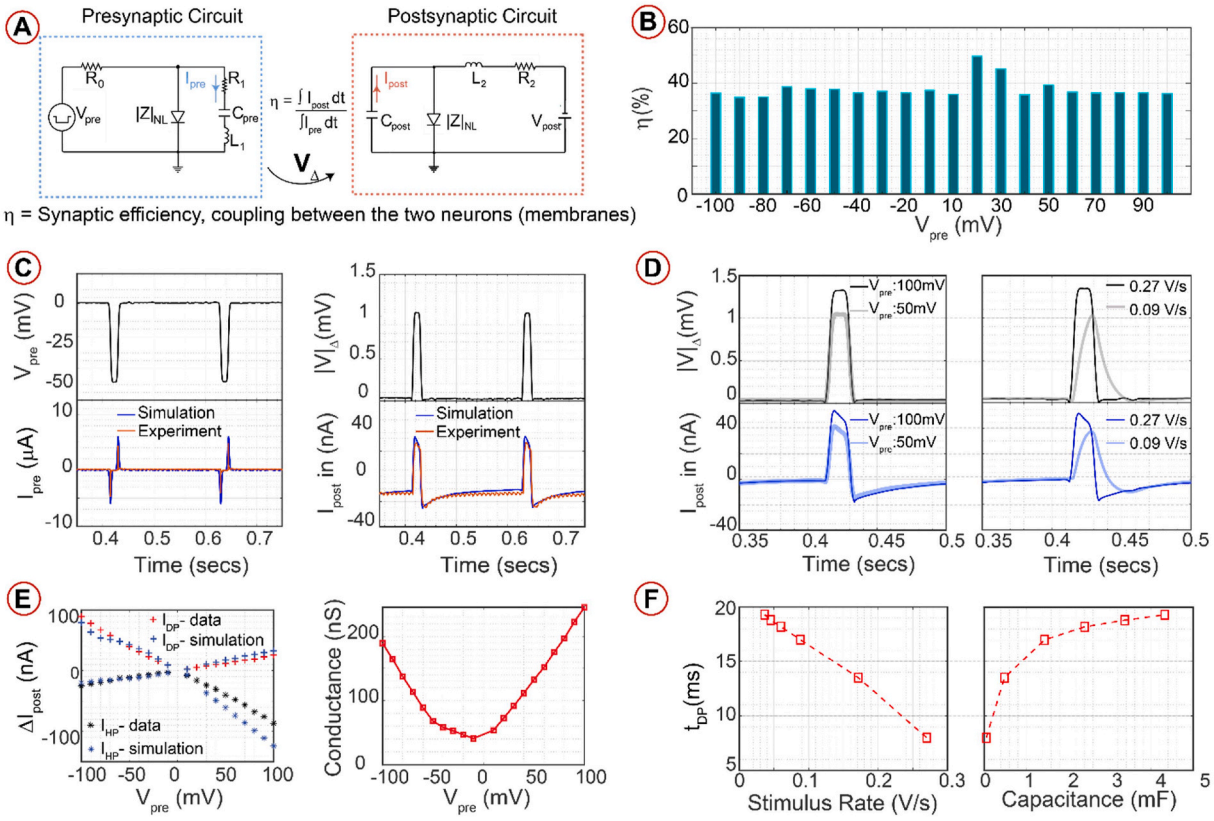

Fig. 2. The synaptic transistor is modeled as a pre-synaptic and post-synaptic neuron as shown in the equivalent circuit diagram (A). The plot (B) shows the synaptic efficiency that couples the pre and post-synaptic elements in the synaptic transistor. The pre-synaptic stimulus and current as observed from experimental data and its comparison to FHN model is shown in (C) (left) for pre-synaptic circuit. The post-synaptic stimulus due to pre-synaptic ion ingress into the cleft is shown in (C) (right) with the post-synaptic activity. The dependence of post-synaptic activity on magnitude and conduction velocity in the pre-synaptic neuron is shown in Figure (D) followed by the comparison of model and experimental data for various magnitudes of pulse stimulation (E) (left) and as a result conductance metric of post-synaptic membrane as a function of pre-synaptic stimulus is shown on (right). The plot (F) shows the dependence of depolarization time (t_{DP}) with stimulus rate and capacitance of pre-synaptic membrane where t_{DP} increases with increasing capacitance of the pre-synaptic membrane and decreasing rate of stimulus in synaptic transistor cleft.

3.2. Animal testing - longitudinal study design and detection of onset and progression

We designed an in vivo longitudinal study to determine the nerve conduction velocity of two animal cohorts with m^+/db and db/db lineage. No statistical methods were used to predetermine sample size. The animals were tagged and grouped randomly using a computer-based algorithm (www.random.org) and both footpads of each group were monitored every 4 weeks. Details on longitudinal study design and animal protocols and lineage can be found in **SI** (section 2.1 & 2.2). Post-anesthetization of animals with isoflurane, a 14G needle-catheter was inserted intramuscularly in the dorsal side of the hind limb in such a way that the catheter was in close proximity to the sciatic nerve. The needle was withdrawn leaving the catheter in place for a ~1 mm synaptic transistor sensor to insert through it. Placement of the transistor sensor in vicinity of the nerve was confirmed by cyclic voltammetry (SI Fig. 12) and ultrasound images of the mice post insertion of the catheter (SI Fig. 13). (Venugopal et al., 2014) These surgical procedures were scheduled such that the same limb of any animal doesn't undergo needle insertion more than once a month. The animals were allowed to recover fully from anesthesia. No complications at the site of catheter insertion or abnormality in gait were observed throughout the study period. In each experimental procedure, the anesthetized mice were electrically grounded on a temperature regulated (37°C) base plate and were thermo-mechanically stimulated utilizing metallic forceps on their footpads once the synaptic transistor sensor was at a steady state. Thermal maps of the mice (Fig. 3A) helped keep track of the temperature during mechanical stimulation. Post-synaptic activity resulting from stimulating the footpads at normal body temperature and in a hypothermic state for m^+/db and db/db at 12 weeks of age is shown in the inset of Fig. 3A. For stimulation at body temperature, the mouse footpad was gently touched with forceps while its temperature was maintained globally at 37^0C using the base plate. For hypothermic stimulation, footpads were initially numbed with ice for 20 s, resulting in a temperature drop to ~10°C, following which the footpads were mechanically stimulated. Fig. 3B summarizes the average t_{DP} of post-synaptic current responses recorded from both groups (m^+/db:n=9; db/db: n=8) in response to thermomechanical stimulation of the footpads as a function of their age. The db/db cohort shows a higher t_{DP} in comparison to m^+/db as early as week 7 and this pattern progressively increases with age. It can also be observed from the right-hand y-axis that the population response progressively decreases in the db/db cohort with age while the same cannot be said for the m^+/db cohort. A complete absence of post-synaptic activity in response to pre-synaptic stimulus was noted in a subset of animals in the db/db cohort over time which led to a global decrease in population response. This absence of activity maybe secondary to axonapathy. Diabetic mice develop neuropathy that causes lower NCV over time due to demyelination or become numb to touch altogether likely due to axonapathy. Hence, the key differences observed in t_{DP} of post-synaptic responses recorded by transistor sensor from m^+/db and db/db groups is (i) higher t_{DP} for responses recorded from db/db than from m^+/db; (ii) Post-synaptic responses recorded at hypothermic state have a higher t_{DP} (~ 4 times) compared to their activity at body temperature ~37°C (waveform progression or a m^+/db

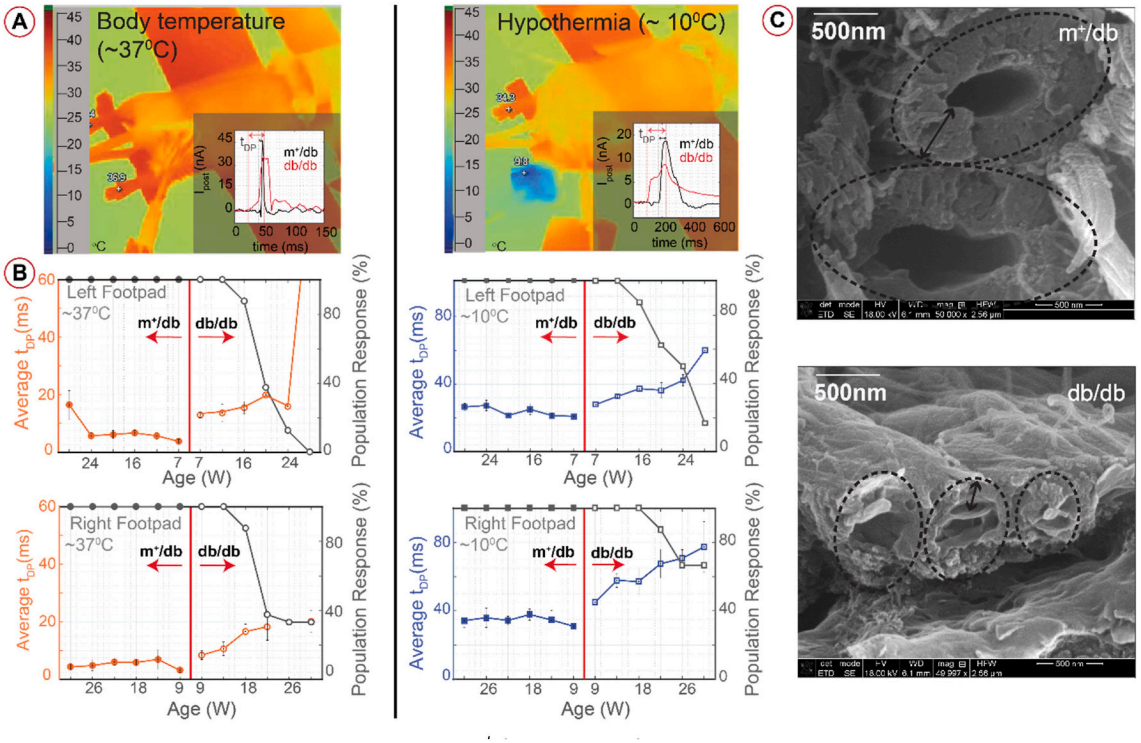

Fig. 3. Progression of neuropathy in m^+/db and db/db mice utilizing synaptic transistor sensor in response to thermomechanical stimulation. (A) Thermal maps of mice at normal body temperature (top) and hypothermia (bottom) prior to mechanical stimulation. The corresponding post-synaptic activity in response to the stimulation is shown for both mice types at normal body temperature and hypothermic states are shown in the insets. (B) Average response of progression of nerve conductivity with age for both mice types at ~ 37^0C (top left for left footpad and top right for right footpad). Similarly, average response of progression of nerve conductivity with age for both mice types at ~ 10^0C is shown in bottom left for left footpad and bottom right for right footpad. (C) Scanning electron micrograph images of sciatic nerve cross-sections of m^+/db (top) and db/db (bottom).

and db/db animal from week 7–24 at both temperature states is shown in SI Fig. 16). At low temperatures, the kinetics of ion transport are slow in the bloodstream which generally lowers NCV and this is reflected in the broad temporal response of post-synaptic currents.

To elucidate the nerve damage visually, scanning electron micrograph images of the sciatic nerve for both groups were captured (Fig. 3C) and compared. It can be observed that the myelin layer thickness (shown in dotted line) is smaller for db/db (bottom) as compared to m^+/db (top). The relationship between axonal diameter and myelin thickness is known to reflect NCV along an axon (Waxman, 1980). The SEM images of the sciatic nerve in diabetic mice revealed thin disrupted myelin sheath and decompaction that is in line with the loss of sensitivity and broad post-synaptic current responses as detected by the *ad hoc* transistor sensors.

Signal attributes of the data collected in the study were integrated into a machine learning framework to develop a polyneuropathy detection model. To develop this model, logistic regression and machine learning concepts were utilized and a probability of neuropathy algorithm was generated. Classification of neuropathy between the subjects (m^+/db and db/db) is done by utilizing the sigmoid function, a special case of logistic function. The goals of the model are to successfully identify subjects with neuropathy and subjects without neuropathy and determine a probability estimate of developing neuropathy over time in each group. Classification of neuropathy in subjects is based on the probability estimate as a threshold, where any subject predicted to have a probability estimate higher than 0.5 is classified as having developed neuropathy for the purpose of training the machine learning (ML) neuropathy model. Upon completion of algorithm training, the optimized weights associated with the input parameters were determined utilizing gradient descent. Determined weights $\theta_0, \theta_1, \theta_2$, help locate the decision boundary to differentiate between the two types of subjects as shown in Fig. 4A. Further details pertaining to the training of the algorithm and determination of the decision boundary are outlined in SI. Electrophysiology data from footpads at body temperature (~37^0C) as acquired at weeks 7 and 9 was used to train the model. A 95% confidence interval of the input parameters (t_{DP} and t_{DP+RP}) was chosen to account for flutter in the data. Utilizing the weights obtained by training the logistic regression neuropathy model, a decision boundary was generated (equation shown below Fig. 4C). The algorithm was tested on data collected from footpads at ~ 37^0C during week 12, week 16 and week 20 from both groups. The algorithm is observed to be predictive, with an average accuracy above 90% (Fig. 4B).

4. Conclusion

We have demonstrated a synaptic transistor-based sensor framework that can be broadly applied *in vivo* for detecting temporal variations of cation fluxes and correlate the measured response to the underlying electrophysiological (or) biophysical process. In this work, we demonstrate the viability of PPy(DBS) based sensor to detect underlying neuronal conduction and correlate it to the progression of polyneuropathy in diabetic mice. While we note that the measured response is not directly the underlying action potential, the readout is an averaged-out response that resembles nerve action potential and allows us to quantify the progressive deterioration of signal conduction in the sciatic nerve. In addition, we demonstrate the procedure required to precisely fabricate the sensor with controlled chemo physical (charge density, filling efficiency) and geometrical properties to perform an *in vivo* longitudinal study. The mathematical model developed to understand synaptic coupling for the synaptic transistor provides the guidance required for designing sensors that can be applied to a wide variety of electrophysiology measurements for research and clinical diagnostics.

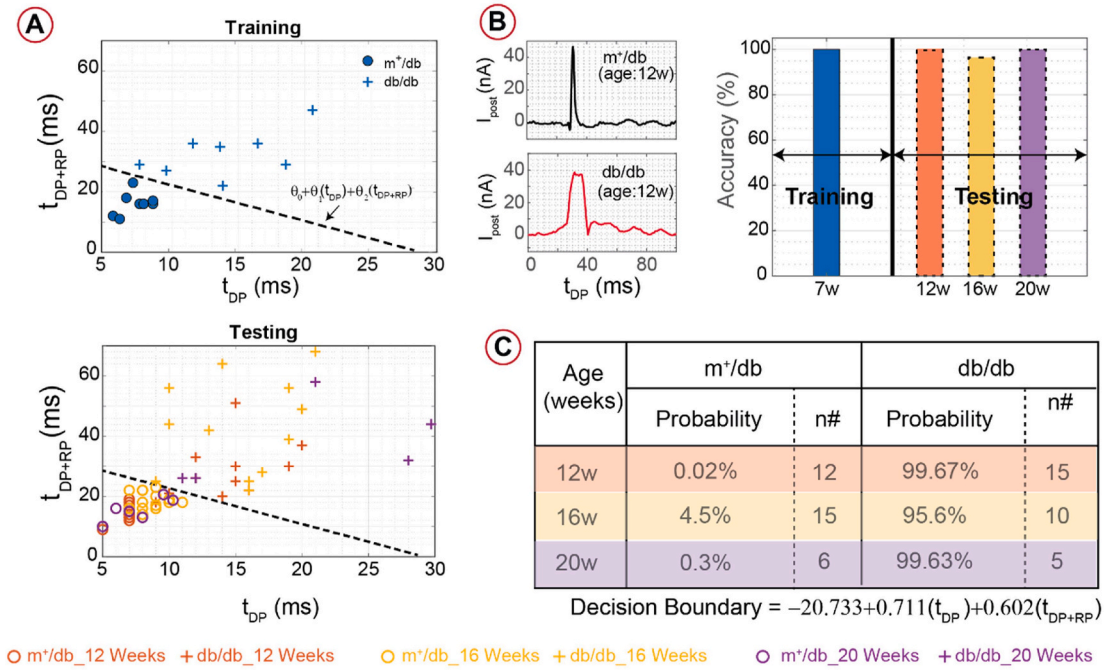

Fig. 4. Probability of neuropathy algorithm (A) Training of the algorithm (top) utilizing week 7 and week 9 data of footpad responses at normal temperature from both groups to locate the decision boundary; testing of the algorithm (bottom) against similar data collected at week 12, week 16 and week 20. (B) Accuracy of algorithm for the train and test data set (right); typical footpad responses recorded at normal temperature from both groups (left). (C) Determination of probability estimate of developing neuropathy over time in each group.

Declaration of competing interest

The authors declare that they have no known competing financial interests or personal relationships that could have appeared to influence the work reported in this paper.

Acknowledgements

Funding: This study was supported in part by the NIH R01 grant NS042617, in part by Lilly Indiana Collaborative Initiative for Talent Enrichment (INCITE) grant to CKS, in part by NIH R01 NS085272 to SK and in part by NSF I/UCRC SVC to VS. VS also acknowledges support from OSU Nano systems lab for electron microscopy support presented in this manuscript.

Appendix A. Supplementary data

Supplementary data to this article can be found online at https://doi.org/10.1016/j.bios.2020.112618.

Author contributions

VS and CKS supervised the research. Sensors were fabricated by SG (OSU) and characterized with support from TH and VS. SG (IU), MEM prepared the animals and performed surgery for sensor placement, glucose measurement, tissue collection. SG(IU) processed tissue samples for electron microscopy. SG (OSU) acquired electrom microscopic images. SG (IU) and SG (OSU) and SK designed the longitudinal study. SG (OSU) collected the data from mice, performed data analysis and developed the classification algorithm with support from VS. SG (IU) and SG (OSU), SK, VS and CKS wrote the manuscript.

Data and materials availability

The protocol to fabricate the sensor, perform animal surgery to insert the sensor and form an ad hoc synaptic transistor are provided in SI. All the data files pertaining to this article is available with the manuscript as a compressed archive with SI.

References

Alshelh, Z., et al., 2016. Chronic neuropathic pain: it's about the rhythm. J. Neurosci. 36, 1008–1018.
Bala, U., Tan, K.-L., Ling, K.-H., Cheah, P.-S., 2014. Harvesting the maximum length of sciatic nerve from adult mice: a step-by-step approach. BMC Res. Notes 7, 714. https://doi.org/10.1186/1756-0500-7-714.
Christensen, M., et al., 2014. The foreign body response to the Utah Slant Electrode Array in the cat sciatic nerve. Acta Biomater. 10, 4650–4660.
Cui, X., Hetke, J.F., Wiler, J.A., Anderson, D.J., Martin, D.C., 2001. Electrochemical deposition and characterization of conducting polymer polypyrrole/PSS on multichannel neural probes. Sensor Actuator Phys. 93, 8–18.
Cui, X., Wiler, J., Dzaman, M., Altschuler, R.A., Martin, D.C., 2003. In vivo studies of polypyrrole/peptide coated neural probes. Biomaterials 24, 777–787.
De Gregorio, C., Contador, D., Campero, M., Ezquer, M., Ezquer, F., 2018. Characterization of diabetic neuropathy progression in a mouse model of type 2 diabetes mellitus. Biol Open 7. https://doi.org/10.1242/bio.036830.
Erdogan, C., et al., 2011. Nerve excitability properties in early preclinical diabetic neuropathy. Diabetes Res. Clin. Pract. 94, 100–104. https://doi.org/10.1016/j.diabres.2011.06.011.
Gallardo, E., Noto, Y.-i., Simon, N.G., 2015. Ultrasound in the diagnosis of peripheral neuropathy: structure meets function in the neuromuscular clinic. J. Neurol. Neurosurg. Psychiatry 86, 1066–1074.
Gallego-Perez, D., et al., 2017. Topical tissue nano-transfection mediates non-viral stroma reprogramming and rescue. Nat. Nanotechnol. 12, 974–979. https://doi.org/10.1038/nnano.2017.134.
Gentet, L.J., Stuart, G.J., Clements, J.D., 2000. Direct measurement of specific membrane capacitance in neurons. Biophys. J. 79, 314–320. https://doi.org/10.1016/s0006-3495(00)76293-x.
Gupta, S., Otero, J.J., Sundaresan, V.B., Czeisler, C.M., 2020. Near field non-invasive electrophysiology of retrotrapezoid nucleus using amperometric cation sensor. Biosens. Bioelectron. 151, 111975 https://doi.org/10.1016/j.bios.2019.111975.
Heise, C.O., Machado, F.C., Amorim, S.C., Toledo, S.M., 2012. Combined nerve conduction index in diabetic polyneuropathy. Arq Neuropsiquiatr 70, 330–334. https://doi.org/10.1590/s0004-282x2012000500005.
Hodgkin, A.L., Huxley, A.F., 1952. A quantitative description of membrane current and its application to conduction and excitation in nerve. J. Physiol. Lond. 117, 500–544. https://doi.org/10.1113/jphysiol.1952.sp004764.
Jacquir, S., Binczak, S., Bilbault, J.-M., Kazantsev, V., Nekorkin, V., 2006. Synaptic coupling between two electronic neurons. Nonlinear Dynam. 44, 29–36.

Kerasnoudis, A., Pitarokoili, K., Behrendt, V., Gold, R., Yoon, M.S., 2015. Correlation of nerve ultrasound, electrophysiological and clinical findings in chronic inflammatory demyelinating polyneuropathy. J. Neuroimaging 25, 207–216.

Kudryashov, N.A., Rybka, R.B., Sboev, A.G., 2018. Analytical properties of the perturbed FitzHugh–Nagumo model. Appl. Math. Lett. 76, 142–147. https://doi.org/10.1016/j.aml.2017.08.013.

Kumar, D., Singh, J., Baleanu, D., 2018. A new numerical algorithm for fractional Fitzhugh–Nagumo equation arising in transmission of nerve impulses. Nonlinear Dynam. 91, 307–317. https://doi.org/10.1007/s11071-017-3870-x.

Luan, L., et al., 2017. Ultraflexible nanoelectronic probes form reliable, glial scar–free neural integration. Sci. Adv. 3, e1601966.

Malik, R.A., 2014. Which test for diagnosing early human diabetic neuropathy? Diabetes 63, 2206–2208.

Northcutt, R.G., Sundaresan, V.-B., 2015. Mechanoelectrochemistry of PPy (DBS) from correlated characterization of electrochemical response and extensional strain. Phys. Chem. Chem. Phys. 17, 32268–32275.

Ruhdorfer, A.S., et al., 2015. Selecting a prospective test for early detection of diabetic polyneuropathy. Microsurgery 35, 512–517.

Schmitz, D., et al., 2001. Axo-axonal coupling: a novel mechanism for ultrafast neuronal communication. Neuron 31, 831–840. https://doi.org/10.1016/S0896-6273(01)00410-X.

Tyler, D.J., Durand, D.M., 2003. Chronic response of the rat sciatic nerve to the flat interface nerve electrode. Ann. Biomed. Eng. 31, 633–642.

Venugopal, V., Zhang, H., Northcutt, R., Sundaresan, V.B., 2014. A thermodynamic chemomechanical constitutive model for conducting polymers. Sensor. Actuator. B Chem. 201, 293–299.

Waxman, S.G., 1980. Determinants of conduction velocity in myelinated nerve fibers. Muscle Nerve 3, 141–150. https://doi.org/10.1002/mus.880030207.

Zhang, Y., Li, J., Wang, T., Wang, J., 2014. Amplitude of sensory nerve action potential in early stage diabetic peripheral neuropathy: an analysis of 500 cases. Neural Regen. Res. 9, 1389–1394. https://doi.org/10.4103/1673-5374.137593.